LA-UR-12-20808
Approved for public release; distribution is unlimited.

Title: Tuning the DARHT Axis-II linear induction accelerator focusing

Author(s): Ekdahl, Carl A.

Intended for: Report

Tuning the DARHT Axis-II linear induction accelerator focusing

Carl Ekdahl

I. INTRODUCTION

Flash radiography of large hydrodynamic experiments driven by high explosives is a well-known diagnostic technique in use at many laboratories, and the Dual-Axis Radiography for Hydrodynamic Testing (DARHT) facility at Los Alamos produces flash radiographs of large hydrodynamic experiments. Two linear induction accelerators (LIAs) make the bremsstrahlung radiographic source spots for orthogonal views of each test. The 2-kA, 20-MeV Axis-I LIA creates a single 60-ns radiography pulse. The 1.7-kA, 16.5-MeV Axis-II LIA creates up to four radiography pulses by kicking them out of a longer pulse that has a 1.6-μs flattop. The Axis-II injector, LIA, kicker, and downstream transport (DST) to the bremsstrahlung converter are described in Ref. [1-5].

Adjusting the magnetic focusing and steering elements to optimize the electron-beam transport through an LIA is often called "tuning." As in all high-current LIAs, the focusing field is designed to be as close to that of the ideal continuous solenoid as physically possible. In ideal continuous solenoidal transport a smoothly varying beam size can easily be found for which radial forces balance, and the beam is said to be "matched" to the focusing field. A "mismatched" beam exhibits unwanted oscillations in size, which are a source of free energy that contributes to emittance growth. This is undesirable, because in the absence of beam-target effects, the radiographic spot size is proportional to the emittance.

Tuning the Axis-II LIA is done in two steps. First, the solenoidal focusing elements are set to values designed to provide a matched beam with little or no envelope oscillations, and little or no beam-breakup (BBU) instability growth. Then, steering elements are adjusted to minimize the motion of the centroid of a well-centered beam at the LIA exit. This article only describes the design of the tune for the focusing solenoids.

The DARHT Axis-II LIA was required to be re-tuned after installing an accelerator cell to replace a failed solenoid in March of 2012. We took advantage of this opportunity to improve the design of the focusing tune with better models of the remaining partially failed solenoids, better estimates of beam initial conditions, and better values for pulsed-power voltages. As with all previous tunes for Axis-II, this one incorporates measures to mitigate beam-breakup (BBU) instability, image displacement instability (IDI), corkscrew (sweep), and emittance growth.

Section II covers the general approach to of design of focusing solenoid tunes for the DARHT Axis-2 LIA. Section III explains the specific requirements and simulations needed to design the tune for the injector, which includes the thermionic electron source, diode, and six induction cells. Section IV explains the requirements and simulations for tuning the main accelerator, which consists of 68 induction cells. Finally, Section V explores sensitivity of the tune to deviations of parameters from nominal, random variations, and uncertainties in values. Four appendices list solenoid settings for this new tune, discuss comparisons of different simulation codes, show halo formation in mismatched beams, and present a brief discussion of the beam envelope equation, which is the heart of the method used to design LIA solenoid tunes.

II. TUNE DESIGN

The design of the solenoidal focusing tune is accomplished using a computer code that solves the second-order differential equations for the beam envelope [6]. The code that we use for tuning both DARHT LIAs is the XTR beam envelope code authored by Paul Allison [7,8]. XTR solves for the beam envelope radius and its first derivative, the envelope divergence, as functions of position. The initial parameters required by XTR at the beginning of the integration are the beam kinetic energy, the beam current, the beam emittance, and the two initial conditions: radius and divergence. The initial beam kinetic energy is that acquired by acceleration through the diode AK gap. Also required is a model of the accelerator which includes locations and values for accelerating gaps, locations and energizing currents for focusing solenoids, and beam tube and aperture sizes. Acceleration is calculated from a thin lens model of the potential in the gaps. The solenoidal focusing field in XTR is calculated from solenoid models that have parameters fit to experimental measurements.

XTR envelope predictions have been extensively compared with experimental results, as well as with the LAMDA envelope code [9,10], the LSP particle-in-cell (PIC) code [11], and the TRAK finite-element ray-trace code [12]. The agreement in all cases was excellent. A few of these comparisons are described in Appendix B for reference. A brief discussion of the beam envelope equation used by XTR and LAMDA is included in Appendix C.

III. INJECTOR SIMULATIONS

The DARHT Axis-II Injector consists of a Marx-generator powered diode with a hot, dispenser cathode, and six induction acceleration cells. Unlike Axis-I, we have no direct measurements of the properties of the beam as it exits the diode, so we must rely on computer simulations of the diode to provide the initial conditions for XTR. All diode simulations were performed in 2-D using the TRICOMP suite of codes[13]. The applied electric and magnetic fields were simulated using finite-element methods based on a conformal triangular mesh model of the DARHT Axis-II diode [14]. The TRAK advanced electron-gun simulator [12] in this suite was then used to simulate the space-charge limited beam current from the thermionic cathode.

The applied electric field in the diode was calculated with the TRICOMP/ESTATcode [13], using an accurate model derived from engineering drawings of the high-perveance geometry in use since 2007. The applied magnetic field was calculated with the TRICOMP/PERMAG code [13], using models of the solenoids in the diode and accelerator cells, including magnetic materials [15]. Initial magnetic field calculations included three injector cells [15], but that has been simplified to a single-cell model, which has an on-axis on axis field less than 0.5% different.

Space-charge limited flow of electrons can result from any source of electrons – thermionic, field-emission, plasma-extraction, photo-emission, or Compton scattering. The maximum current that can be drawn from any of these sources is limited by the space charge of the resulting beam. When the current is space-charge limited, excess electrons from the source are reflected back to the emission surface by the space-charge potential well. Child [16] and Langmuir [17] both derived the familiar space-charge limited current $I \propto V_{AK}^{3/2}$ law for infinite-planar, non-relativistic diodes (Child for ions and Langmuir for electrons), but it was Langmuir who accounted for the reflected electrons [18].

Space-charge limited current in TRAK is self-consistently calculated by iteratively increasing the current from emission elements until the total electric field at the surface is zero.

This is the Child condition [16], and it actually occurs at the surface where excess emitted electrons are reflected, rather than exactly at the emitter, as explained by Langmuir, who also showed that this surface is only slightly displaced from the emitter itself (less than $16\mu\text{m} \times (T(\text{K})/1000)^{4/3} / \sqrt{1000 \times J(\text{A/cm}^2)}$)[18]. This is less than 1 micron for the >5-A/cm^2 DARHT thermionic cathode at <2000K, and is ignored in the simulations. The iterative algorithm in TRAK for calculating the space-charge limit converges in about~7 iterations, and varies only slightly with further iterations. To reduce the uncertainty in the result, I run all problems for a total of 20 iterations.

Figure 1 illustrates the TRAK simulation of the DART Axis-II high-perveance diode, showing the equipotentials and the space-charge limited electron beam. The initial conditions for XTR were determined from TRAK at ~80 cm downstream from the cathode surface, at Z = 100 cm. The initial conditions, the space-charge limited current, and the normalized emittance were obtained at that position from simulations with AK voltages ranging from 100 kV to 2.8 MV, so that XTR could be used to predict beam behavior during the long, ~500–ns risetime.

The XTR initial values supplied by TRAK are based on our beam position monitor (BPM) measurements of beam current, which are less uncertain than measurement of the diode AK voltage with our capacitive voltage monitor. Averaging a random selection of 9 shots during our last day of operation before maintenance (2/16/12) gave a beam current of 1.69 kA (2.3% standard deviation). This would have been produced in a TRAK simulation with V_AK = 2.2 MV, which is within 5% of the measured 2.1 MV. Since the calibration of the diode voltage measurement is believed to be at least 5% uncertain, I used the more accurate current measurement to establish the initial values from TRAK simulations, which are given in Table I.

Table I. Beam initial parameters from TRAK simulation.

Quantity	Symbol	Value	Units
Location	z	100	cm
Beam Current	I_b	1.68	kA
Diode AK Voltage	V_{AK}	2.20	MV
Normalized Emittance	ε_n	178	π-mm-mr
Initial Conditions :			
Envelope Radius	r_0	8.80	cm
Envelope Convergence	r_0'	24.74	mr

XTR also requires the beam-loaded accelerating cell potentials. For these simulations I used values that were also based on data from 2/16/12. Each XTR cell potential was the average of the same 9 beam shots used to establish the initial values for XTR. Each of the 9 values was itself an average over 200 ns beginning at 3.0 μs, which is well into the flattop region of the current pulse. The pulsed power was very stable; the standard deviations of the 9-shot averages were less than 0.3% on that date.

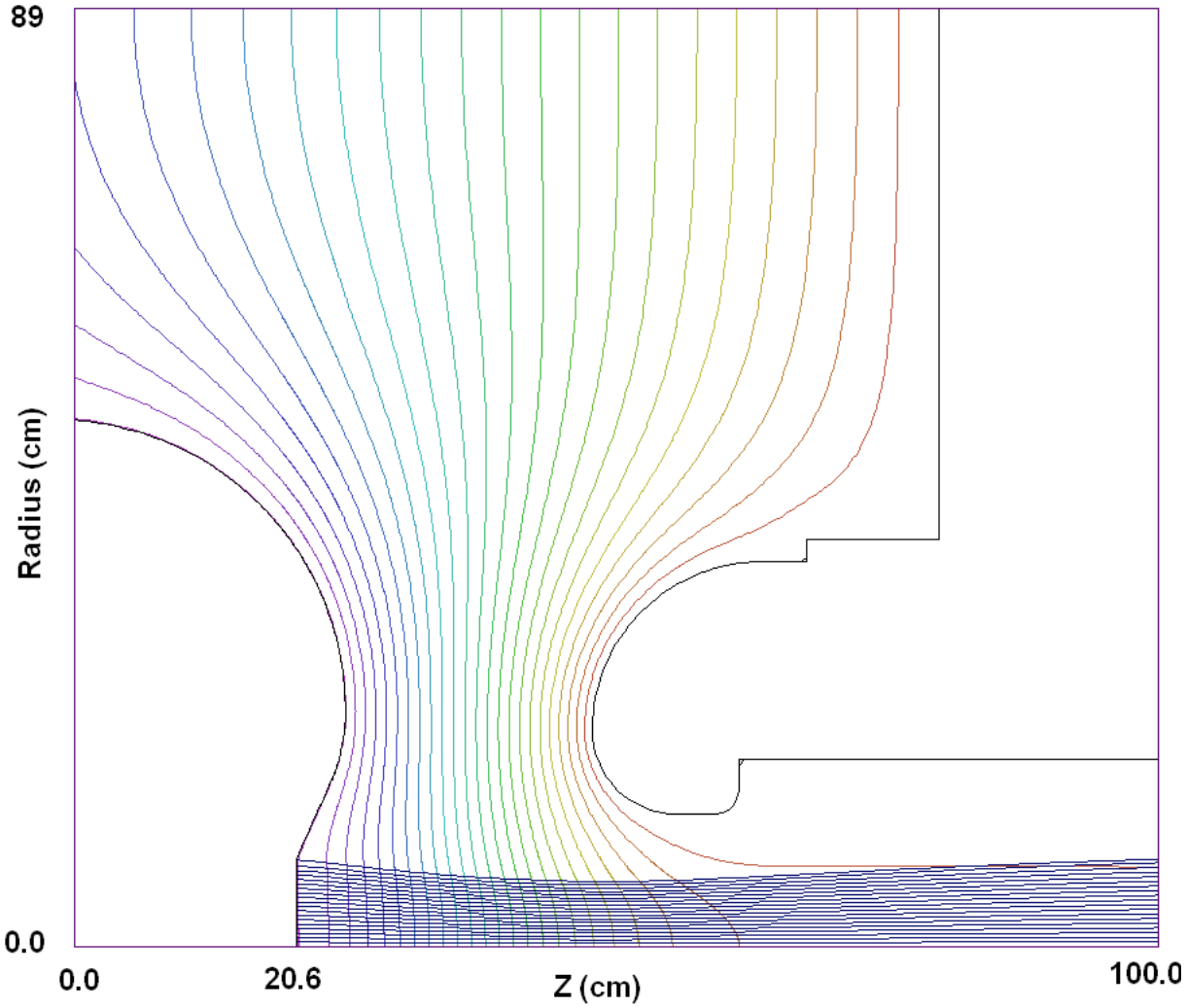

Figure 1: TRAK simulation of space-charge limited current emitted by the hot dispenser cathode in the Axis-II high-perveance diode. The initial conditions for the envelope codes are obtained at the right hand edge of this plot.

There was no need to redesign the solenoid tune for the injector. Even with the new, improved initial values and cell voltages; the present tune meets all requirements. These are:

1. The magnetic flux linking the cathode must be minimized with the reverse polarity "bucking coil."
2. The solenoidal field used in XTR must agree with the field used by TRAK in the diode region.
3. The off-energy beam head must transport through the injector solenoids, even if the cell accelerating voltages fail.
4. The average magnetic field in the injector cells must be greater than ~100 Gauss to suppress BBU and IDI.
5. The XTR integrations must begin far enough downstream into the beam pipe that the applied diode field is much less that the space-charge field of the beam.

1. The magnetic flux linking the cathode must be minimized with the reverse polarity "bucking coil." The thermionic source emission has no coherent angular motion, so the canonical angular momentum there is only proportional to the magnetic flux linking the cathode. The canonical angular momentum adds in quadrature to the beam emittance to determine the radiographic spot size. Therefore, the DARHT diodes incorporate reversed polarity "bucking coils" to minimize this flux.

2. The magnetic field used in XTR must agree with the field used by TRAK. This is required to ensure that the XTR simulations are self-consistent with the TRAK simulations providing the initial conditions for XTR. Equivalence of the magnetic fields was achieved by iteratively alternating TRAK and XTR runs while varying the solenoidal fields in both to simultaneously satisfy the other constraints in this list. The magnetic fields on axis at completion of this iterative process are plotted in Fig. 2, which shows the agreement between the fields models used for injector simulations with TRAK (ray trace), LSP (PIC), and XTR or LAMDA (envelope) codes.

3. The off-energy beam head must transport through the injector solenoids, even if the cell accelerating voltages fail. The solenoids are interlocked, as are the pulsed-power charging supplies. However, cells can fail due to other causes, so the transport must be robust enough to prevent beam spill beam if this happens. Loss of beam electrons onto a cell insulator during, or just before, the high-voltage pulse can result in flashover or arcing across the insulator. Beam transport without loss is illustrated in Fig. 3, which shows the beam envelope for V_AK=0.9 MV. This is the least matched part of the beam head, and produces the largest beam envelope excursion in the injector cells. Even with no voltage on the accelerating cells the 0.9-MeV beam slice never spills on the injector cells; it only scrapes the beam tube after leaving the injector cell block.

4. The average magnetic field must be greater than ~100 Gauss. This is required to suppress BBU and IDI, which have growth rates strongly suppressed by the magnetic field strength. IDI also has a stability threshold at ~100 Gauss for our beam current.

5. The XTR integrations must begin far enough downstream into the beam pipe that the applied diode field is much less that the space-charge field of the beam. The only applied electric fields modeled in XTR are those of the accelerating cells, so the XTR simulation must begin in a region where there are no other applied electric fields. The field applied to the diode is strongly attenuated in the beam tube, and locating the initial point for XTR far enough into the tube that the space-charge field dominates is sufficient. This has been extensively tested by comparing XTR simulations starting at different locations against TRAK and LSP simulations, which account for all electric fields.

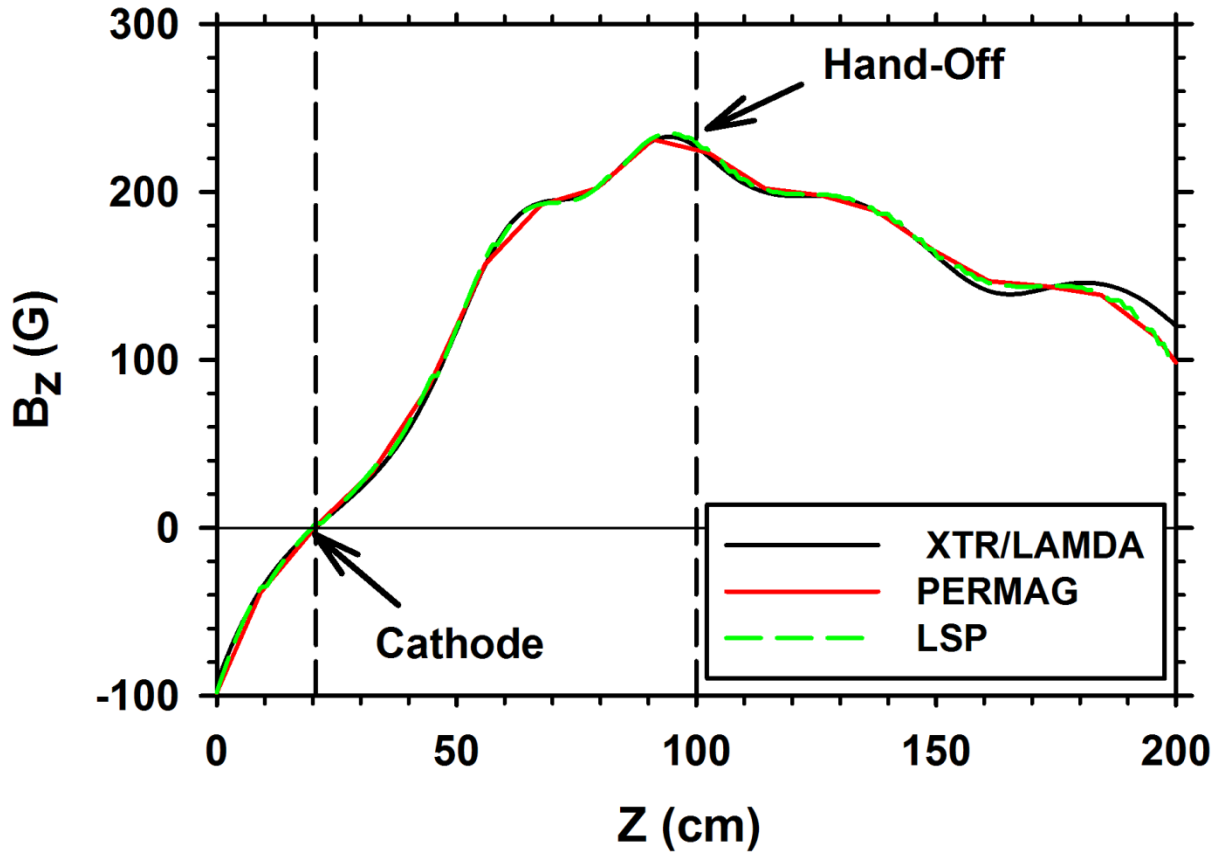

Figure 2: Comparison of Bz on axis used in the several codes used for design of the injector tune. The position of the cathode is indicated by the vertical dashed line at Z = 20.64 cm. The location where the initial conditions of the beam envelope (radius and convergence) are handed off from the diode simulations to the envelope code is also indicated by the vertical dashed line at Z = 100 cm. The black line is the field from solenoid models used in the XTR or LAMDA envelope simulations. The red line is the field from PERMAG, which was used for the TRAK ray-trace simulations. The dashed green line is the field used for the LSP particle-in-cell simulations of the diode.

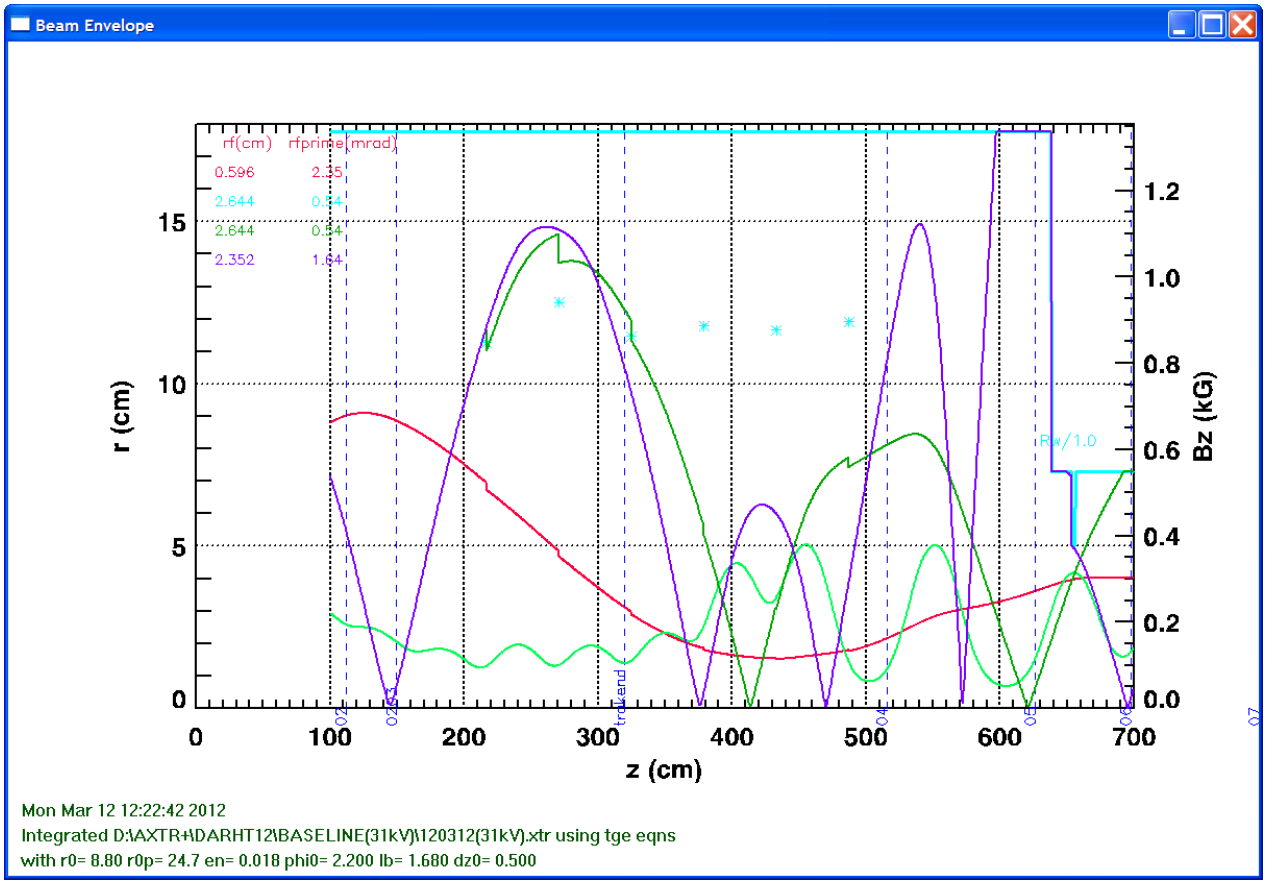

Figure 3: Beam transport through the injector cell block and into the BCUZ as simulated by XTR. The solenoidal magnetic field strength on axis is denoted by the light green curve (legend on right). The red curve is the beam envelope during the 1.68-kA, 2.2-MeV flat-top of the diode pulse. The dark green curve is the envelope at the instant during the risetime when the diode voltage is 0.9 MV, producing 480 A. The purple curve is the beam envelope for that same instant when there are no accelerating cell potentials. Note that in this last case the beam scrapes the beam tube, shown in blue, but only after leaving the injector cell block.

Figure 3 also illustrates the characteristic, unavoidable necking of the beam envelope during the flattop (red curve). This results from any tune that meets the requirements in the preceding list. Since there are significant gaps in the solenoidal spacing in the beam-head cleanup zone (BCUZ), it is impossible to capture and transport this smaller beam, so it is allowed to expand through this zone, and then refocused in the main accelerator.

The simulations of the beam produced by the diode and injector cells have been experimentally validated over a wide range of beam parameters. We have no direct measurements of the properties of the beam as it exits the diode, so we must rely on TRAK gun-design simulations of the diode to provide the initial conditions for XTR or LAMDA envelope codes. One way to experimentally confirm this procedure is to measure the current passed through an aperture by the off-energy beam head, which has a continuously varying envelope. This causes a time dependent variation of the transmitted current, and the procedure is valid to the extent that the envelope calculation using TRAK initial conditions agrees with the experimental data. Figure 4 shows such a comparison. The agreement between theory and experiment seen in the figure lends confidence in using TRAK to establish initial conditions for the envelope codes.

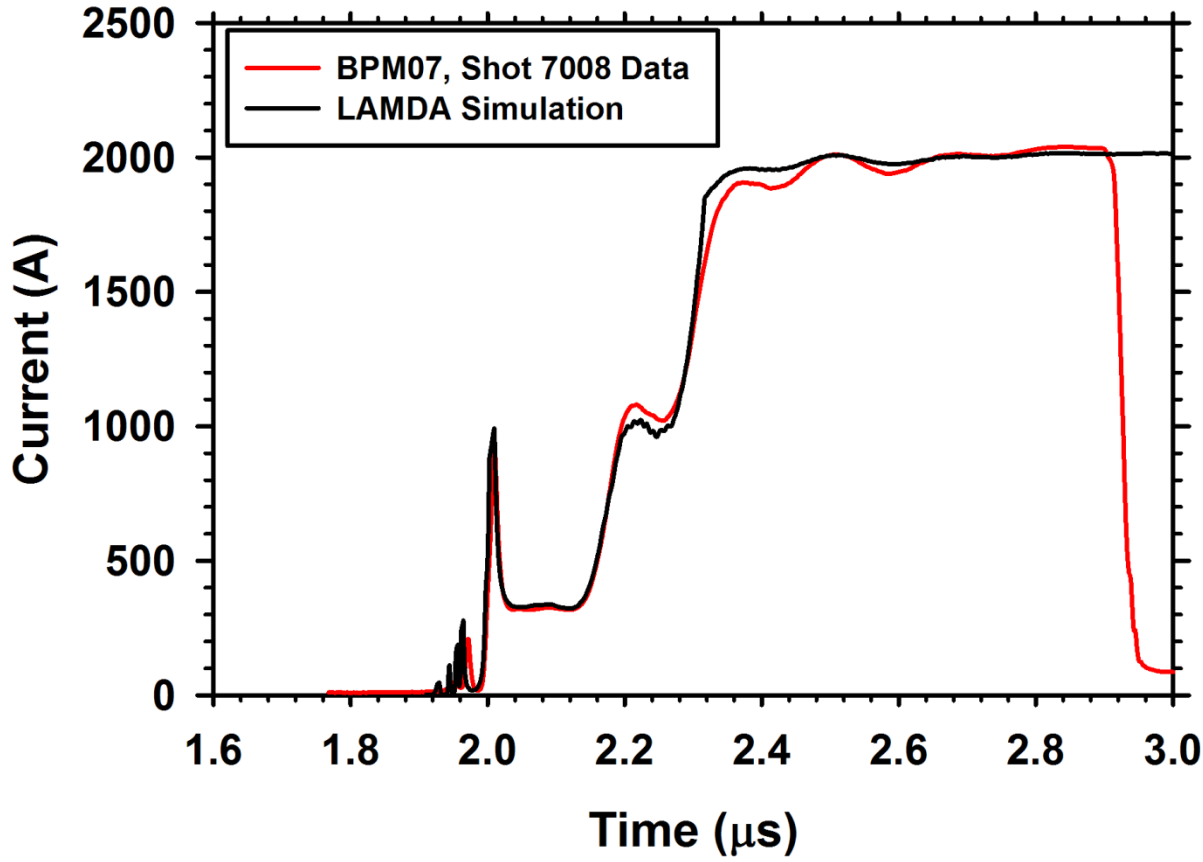

Figure 4: Current transmitted through the BCUZ for the cleanup tune. The shorter pulse (shown in red) is data from shot 7008 from the first BPM beyond the BCUZ apertures. The longer pulse (shown in black) is the result of the LAMDA simulation. The LAMDA simulation used initial conditions derived from TRAK simulations of the diode.

IV. MAIN ACCELERATOR SIMULATIONS

XTR was used to design a new tune through the main accelerator. The existing tune for the injector and BCUZ was unchanged, because it met all requirements using the improved estimates for initial conditions at the diode exit (Table I). I designed new tune for the main accelerator using improved values for defective solenoids, and measured values for beam loaded cell voltages.

The magnetic fields in the XTR simulations were calculated from ideal solenoid models having parameters fit to experimental measurements. For most of the solenoids the nominal parameters are based on Tim Houck's data [25]. There are 7 solenoids known to be defective (21,24,26,43,67,72,73). These have experimentally measured resistances (R=V/I) less than the nominal 12.2 Ω [26]. We presume this is the result of shorted turns. To model these in XTR, I also presume that the shorting does not change the effective length or diameter of the magnet, so can be accounted for by simply adjusting the sensitivity (Gauss/Amp). Data from 2/16/12 was used to calculate the required adjustment for the defective magnets (Table II), and these models were then used in design simulations for this tune.

Table II. Defective Solenoids

cell	shot 17047	shot 17046	shot 17044	mean	% of 12.17
21	10.35	10.35	10.37	10.36	85.10
24	11.19	11.2	11.22	11.20	92.06
26	11.35	11.36	11.37	11.36	93.34
43	10.34	10.36	10.37	10.36	85.10
67	7.44	7.46	7.46	7.45	61.24
72	11.38	11.41	11.42	11.40	93.70
73	10.11	10.14	10.15	10.13	83.26

The beam-loaded accelerating cell potentials in the XTR simulations were based on data from 2/16/12. Each cell voltage was the average of the same 9 beam shots used to establish the initial values for XTR. Each of the 9 values was itself an average over 200 ns beginning at 3.0 μs, which is well into the flattop region of the current pulse. Standard deviations of the 9-shot averages were less than 0.3% on that date.

The solenoidal magnet settings for the new accelerator tune (120312) are given in Appendix B, and the resulting beam envelope is shown in Fig. 5. Here one sees the beam entering the main accelerator after expanding in the BCUZ. After entering the accelerator, the beam is focused down to a radius matched to the strong magnetic field needed to suppress the BBU instability. The beam is then transported to the exit using little change in the average focusing field. The three significant gaps in the focusing field (~3.5 m, ~4.4 m, and ~4.7 m) result from lack of inter-cellblock solenoids to bridge the inter-cellblock gaps. The last two of these gaps is especially problematic. Since the gap spacing is nearly in resonance with the envelope oscillation frequency, an oscillation can be parametrically excited.

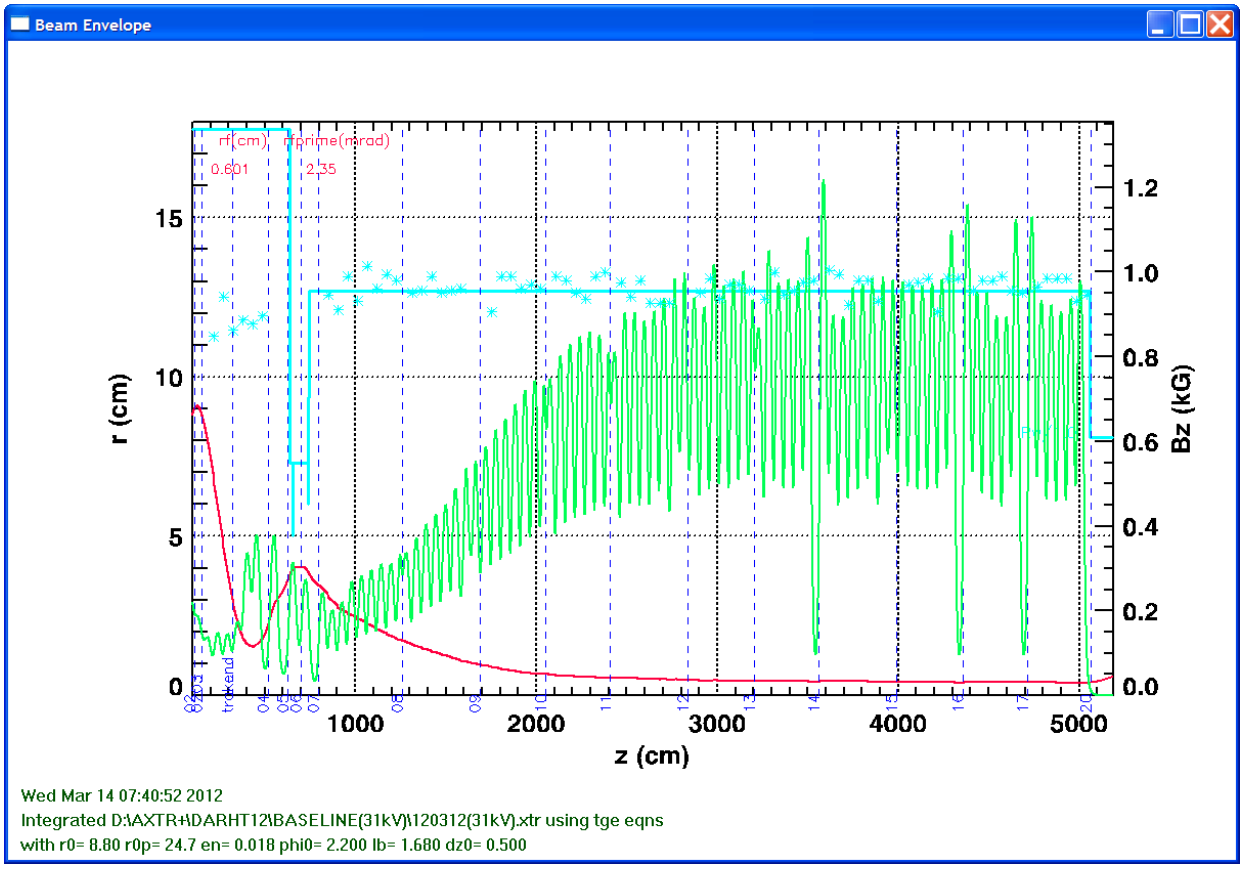

Figure 5: XTR simulation of beam transport through the DARHT Axis-II LIA. The solenoidal magnetic field strength on axis is denoted by the light green curve (legend on right). The red curve is the beam envelope during the 1.68-kA, 2.2-MeV flat-top of the diode pulse. The cell accelerating potentials are shown as cyan asterisks (not to scale). The beam tube wall is indicated by the solid cyan line, and positions of the BPMs are denoted by the vertical dashed purple lines.

Although the LIA solenoidal field varies in z significantly, as much as +/- 25% with cell spacing periodicity, this has little effect on the beam envelope. The characteristic length over which the envelope can respond to changes in solenoidal fields is the betatron wavelength, which is much longer than the cell spacing, so the envelope cannot follow the cell-to-cell field variations. Thus, the envelope dynamics are dominated by the effective focusing field shown in Fig. 6, which has the cell periodicity filtered out. The lack of solenoids between the last cell blocks clearly stands out, showing that these are indeed a problem for the stiff beam in this region.

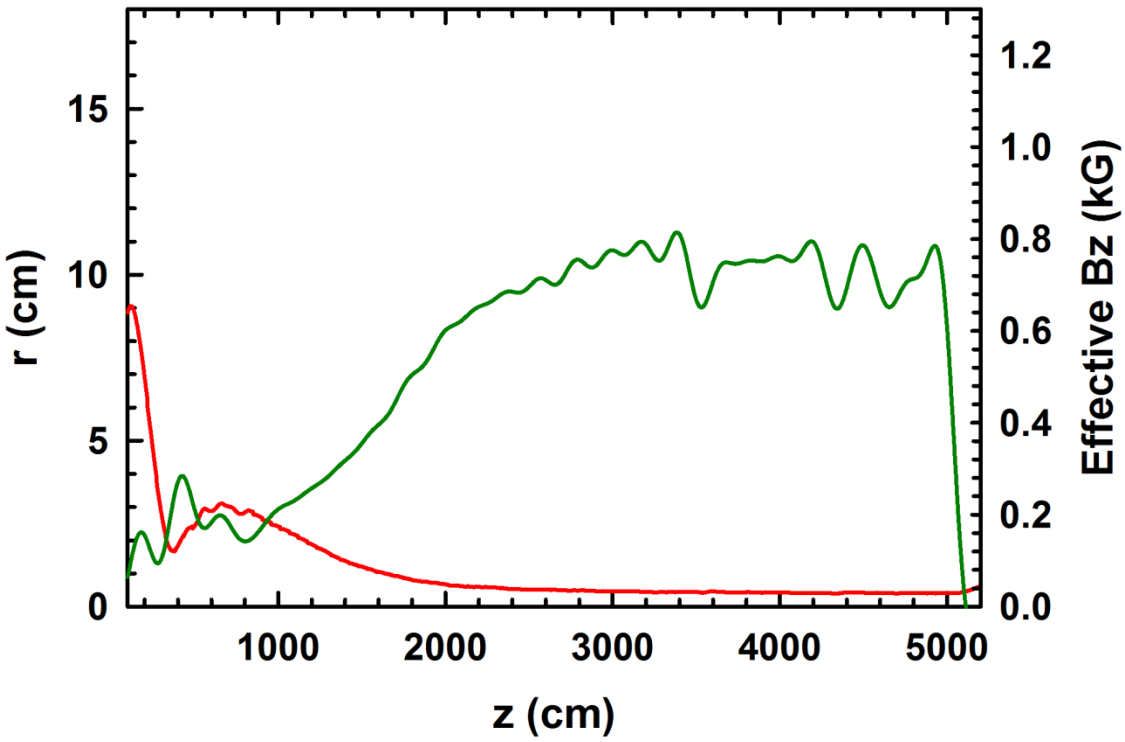

Figure 6: Beam envelope (red curve) and effective solenoidal focusing field (green curve), which is the field shown in Fig. 5 with the cell periodicity filtered out.

This tune satisfies the following requirements:

1. Transport the off energy beam head through the accelerator without loss.
2. Produce a matched beam (no envelope oscillations) during the current flat top.
3. Suppress the BBU to less than 2% of the beam envelope radius.
4. Minimize the corkscrew motion.

1. Transport the off energy beam head through the accelerator without loss. Due to our discovery of problems in the diode when the BCUZ is tuned to scrape off the beam head, we have not used the BCUZ in that mode for a number of years. Therefore, just like the injector, the accelerator tune must transport the entire beam head, because loss of beam electrons onto an accelerator cell insulator during, or just before, the high-voltage pulse can lead to flashover or arcing across the insulator. This tune transports all of the off-energy electrons in the beam head cell high-voltage pulse by taking advantage of the energy gain and the electrostatic focusing provided by the cell potentials. However, with no cell voltages, even the beam flattop will be scraped off after cell block 8. This means that, just like the previous tune, there will be significant beam spill after the cell high-voltage pulse if the crowbar fails to chop off the current pulse. This also sets a requirement for the relative timing between the diode and cell pulses; the optimum is for the 10% of rise times to be the same for the cells and the diode voltage, retarding the cell timing more than ~100ns from this optimum has been shown to result in loss of beam head in the accelerator.

2. Produce a matched beam little or no envelope oscillations during the current flat top. A badly mismatched beam exhibits large envelope oscillations, sometimes called a “sausage,” “m=0,” or “breathing” mode (Fig. 7). The free energy in these oscillations feeds the growth of emittance [19]. The detailed mechanism of this contribution to emittance growth is parametric amplification of electron orbits that resonate with the envelope oscillation, expelling those electrons from the beam core into a halo [21,22].

Another well-known contributor to emittance growth in solenoidal focusing systems is cumulative spherical aberration [19,31], which also over-focuses the edge of the beam, producing hollow beam profiles [33]. However, even though the cumulative spherical aberration is large in our LIA, and the resulting edge focusing is evident in PIC simulations, the resulting emittance growth is small because the beam is rapidly focused to a size much smaller than the bore of the solenoids. Essentially all of the emittance growth observed in PIC code simulations appears to come from the parametric amplification of orbits, so I emphasize matched beam envelopes in the design of tunes.

This new tune also has the built in capability to easily re-match a beam that is initially mis-matched. The first few solenoids in the main LIA matching section (cell block 2) can be used to significantly reduce the oscillations, and subsequent emittance growth, with a procedure much like the “tuning V” we use to minimize beam sweep. This only requires an “emittance meter” at the exit of the accelerator, such as an OTR monitor at station A. Figure 7 shows how gang-tuning those few solenoids can suppress the envelope oscillations of an initially mismatched beam.

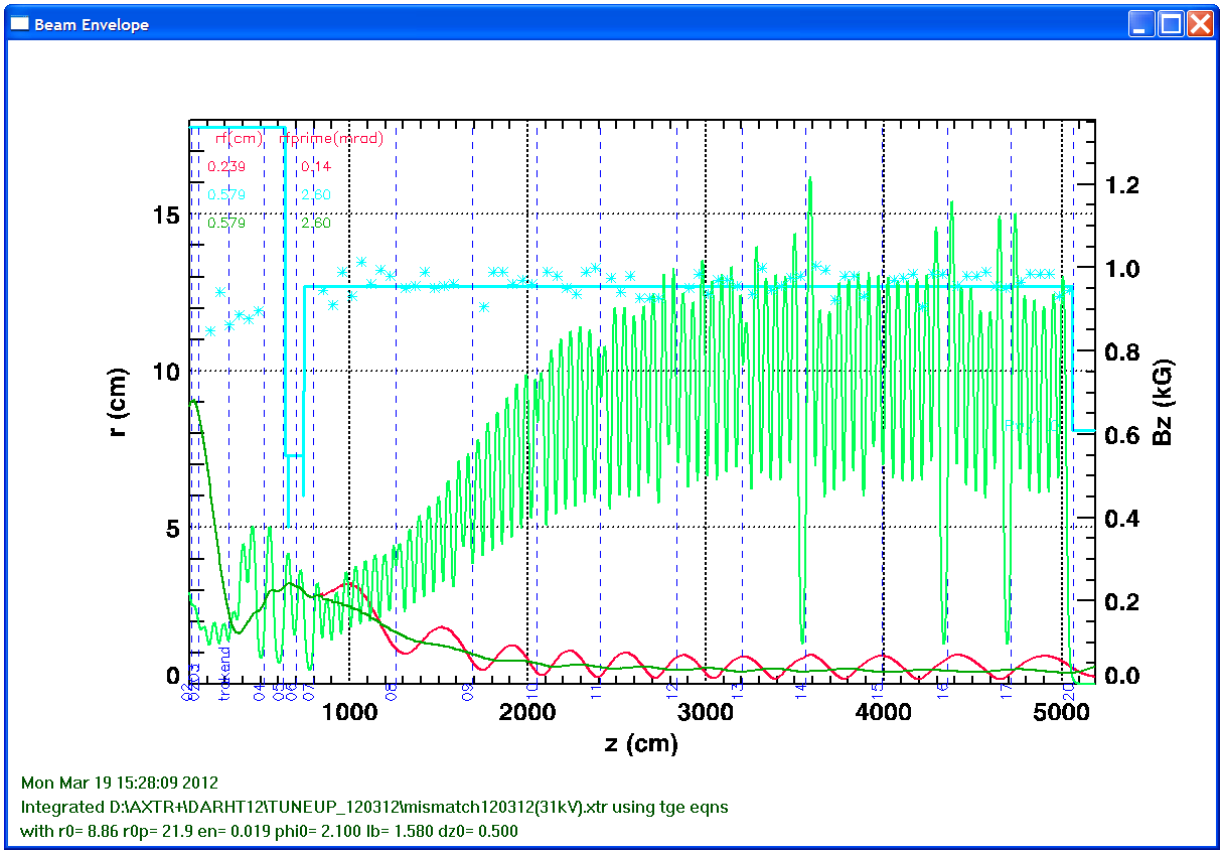

Figure 7: XTR simulation of a mismatched beam (red curve) caused by initial conditions consistent with 1.58-kA diode current (instead of the measured 1.68 kA). This beam was

approximately re-matched (dark green curve) by adjusting only the first three solenoids of cell block 2.

Emittance growth is calculated using LSP PIC code simulations that model a slice of the beam as it transports through the accelerator. Two slice models have been used; Slice "1D" models a centered beam in cylindrical coordinates [20], and Slice "2D" uses Cartesian coordinates to be able to simulate the motion of the beam centroid. Appendix B includes comparisons of the two versions of slice, and comparisons of slice with XTR envelope calculations. I used Slice1D to calculate the growth of emittance in a mismatched beam for this tune. A comparison of the matched-beam envelopes calculated by Slice and XTR is shown Fig. 8. The PIC calculation produces an ~30% larger beam at the exit, because of the relaxation of the initial hard edge profile.

There is no discernible emittance growth in the main accelerator for this matched beam, even though there is appreciable cumulative spherical aberration. The only growth from the initial emittance at the diode is ~10% increase in the injector cells, where the beam is large.

There is also no discernible emittance growth for a matched beam that is initially offset by as much as 1 cm. The ensuing helical motion through the solenoidal guide field does not appear to contribute to emittance growth, at least in these PIC code simulations.

However, there can be significant increases in the emittance if the beam is mismatched. Figure 9 shows the growth of emittance in a mismatched beam, which is accompanied by damping of the envelope oscillations as oscillation energy is randomized. The detailed mechanism of emittance growth is parametric amplification of resonant electron orbits, expelling them from the beam core into a halo [21,22]. This is clearly seen in the phase-space plots from Slice simulations (see Appendix D).

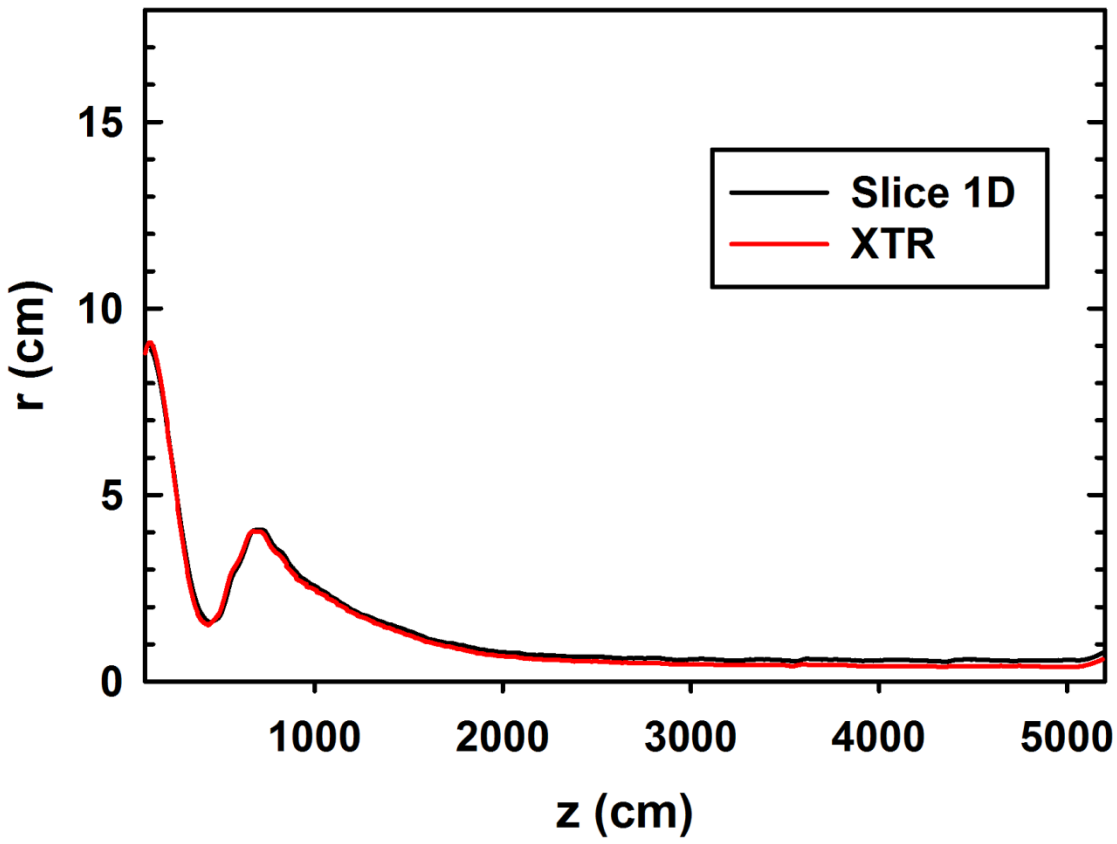

Figure 8: equivalent beam envelope radius calculated by the particle-in-cell code Slice 1D in cylindrical coordinates (black curve) compared with the envelope radius calculated by the XTR envelope code. The radius from the PIC simulation is an equivalent envelope, which is the rms radius of the current distribution multiplied by $\sqrt{2}$.

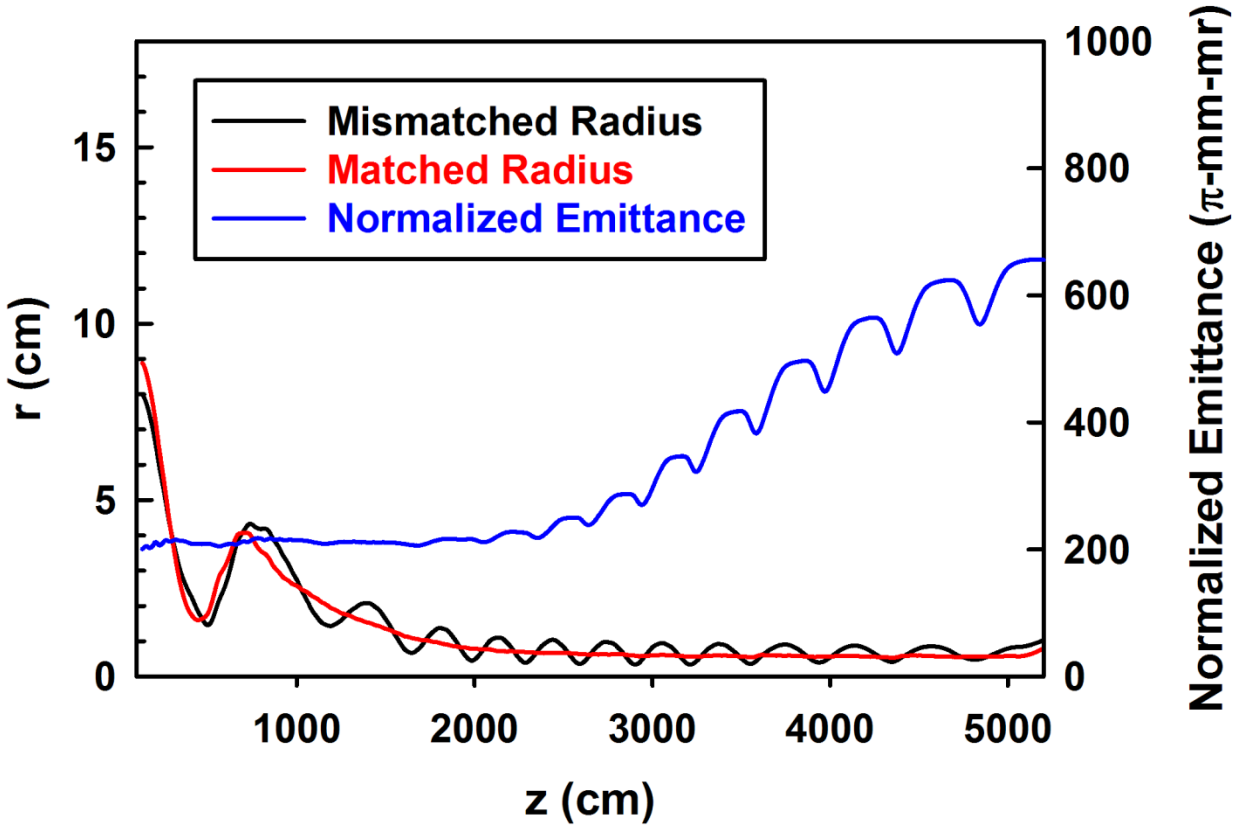

Figure 9: Equivalent envelope of a mismatched beam (red curve) and emittance growth (black curve) as simulated by the Slice 1D PIC code.

Finally, Fig. 10 shows the dependence of the emittance growth on the amplitude of the envelope oscillations. Since the emittance growth relies on the free energy of the oscillations, one might expect at least a quadratic relation of growth to amplitude. Indeed, an empirical fit to the simulations yields the interpolating formula $\varepsilon_n = 210 + 1.4\text{E}3\left(A - 0.29\right)^{2.8}$ π-mm-mr, where the peak-to-peak amplitude is $A = 2(r_{\max} - r_{\min}) / (r_{\max} + r_{\min})$. There was little or no discernible growth for $A < 0.3$, which appears to be a threshold for emittance growth in these Slice simulations. This formula enables one to predict emittance growth based on mismatched beam envelope oscillations predicted by envelope codes, without having to run the time intensive Slice codes for every case. Moreover, if envelope oscillation amplitudes were ever to be experimentally measured, resulting emittance growth could be estimated. Conversely, envelope oscillation amplitudes might be inferred from measurements of emittance growth.

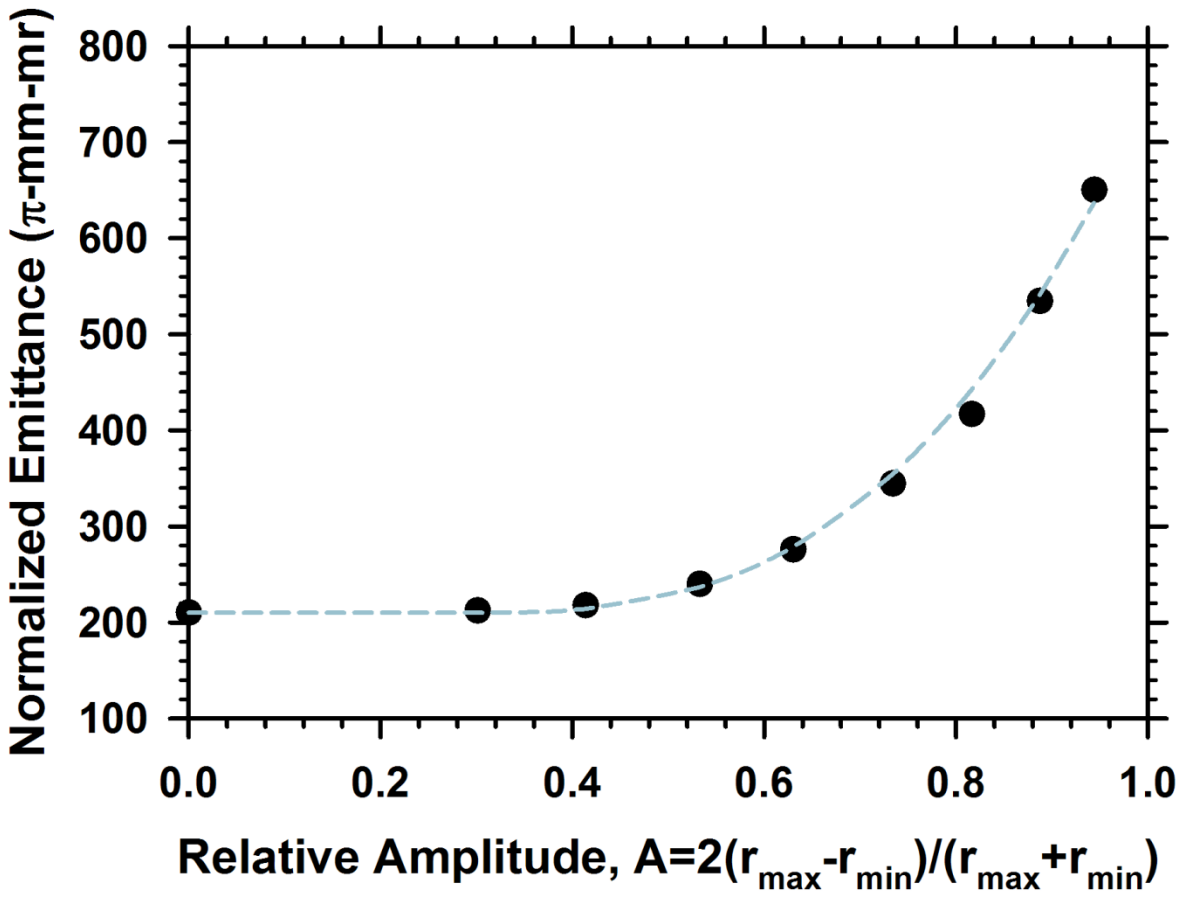

Figure 10: Emittance at the exit of the LIA (z ~ 52 m) as a function of the envelope oscillation amplitude near the beginning of observable growth (z ~ 31 m). The light blue dashed line is the interpolating function $\varepsilon_n = 210 + 1.4\text{E}3\left(A - 0.29\right)^{2.8}$.

3. Suppress the BBU to less than 2% of the beam envelope radius. In the strong focus, weak accelerating gradient DARHT Axis-II LIA, the maximum BBU amplification of an initial perturbation with amplitude ξ_0 is [23]:

$$\xi(z) = \xi_0 \sqrt{\gamma_0 / \gamma}\, \exp\left(I_b N_g Z_\perp \left\langle 1/B_z \right\rangle / 3\times 10^4\right) \qquad (1)$$

Here, I_b is the beam current in kA, N_g is the number of gaps, the transverse impedance $Z_\perp$ is in Ω/m., and $\left\langle 1/B_z \right\rangle$ is in kG^{-1} (the brackets $\langle\ \ \rangle$ denote averaging from the entrance to *z*). We have validated this theoretical formula with experiments on the DARHT Axis-II LIA [3], and used it to design our tunes. These had BBU amplitudes at the exit of <60 microns for the 150-MHz mode[4], which meets the 2% requirement. The number of gaps and transverse impedance in the maximum growth exponent are fixed, so our practical control of growth is through the product $I_b \left\langle 1/B_z \right\rangle$. For the data reported in ref. [4] $I_b \left\langle 1/B_z \right\rangle = 1.91\text{G/A}$ (see Table II). Therefore, ensuring that this product is less than 1.91 G/A for this new tune would keep the BBU amplitude < 60 microns at the exit. Since we are now operating at a reduced diode voltage, I took

advantage of the lower current to reduce the magnetic focusing field in order to reduce the corkscrew, while still retaining sufficient $I_b\langle 1/B_z\rangle$ to suppress BBU. This new tune has $I_b\langle 1/B_z\rangle = 1.85\,\mathrm{G/A}$, which should keep the BBU amplitude to less than 60 micron.

Table II. Tune stability parameters

Tune Name	Start Date	first shot	Ib	<1/B>	Ib<1/B>	<B>
			kA	kG^{-1}	A/G	Gauss
091211B	01/07/10	11293	1.85	1.025	1.90	645
110518(31)	05/19/11	14576	1.68	1.019	1.71	659
120312(31)	04/02/12		1.68	1.100	1.85	614

4. Minimize corkscrew motion. Corkscrew is caused by interaction of beam energy variations with accidental magnetic dipoles resulting from solenoid misalignment [24]. Corkscrew manifests itself in the Axis-II LIA as beam sweep at the exit [4]. Since the dipole strengths are proportional to the solenoid field strengths, corkscrew can be reduced by reducing the focusing field. Thus, the average focusing field should be only strong enough to achieve a reduction of BBU to meet requirement number 3. As mentioned in the discussion of that requirement, our reduced current provided the opportunity to reduce the solenoidal field without effecting the BBU, which should also reduce corkscrew. The average guide field was reduced from 644 G to 614 G. This doesn't seem like much, but the reduction is largely in the region preceding the dipoles we use for tuning V control of the sweep, so it should reduce the required dipole strength.

V. SENSITIVITY TO MACHINE VARIATIONS

A. Diode Performance Variations

The beam current measurements upon which the diode initial conditions were based are +/-2% uncertain. Since this tune was designed for a 1.68-kA beam and the initial conditions for that current, this uncertainty could result in a mismatched beam if the current (and initial conditions) were actually different by as much as 2%. This is illustrated in Fig. 11, which shows the envelopes for the resulting mismatched beams. The mismatched oscillations have relative peak-to-peak amplitude $A \sim 50\%$, which would result in emittance growth less than ~20 π-mm-mr, according to the Slice simulations.

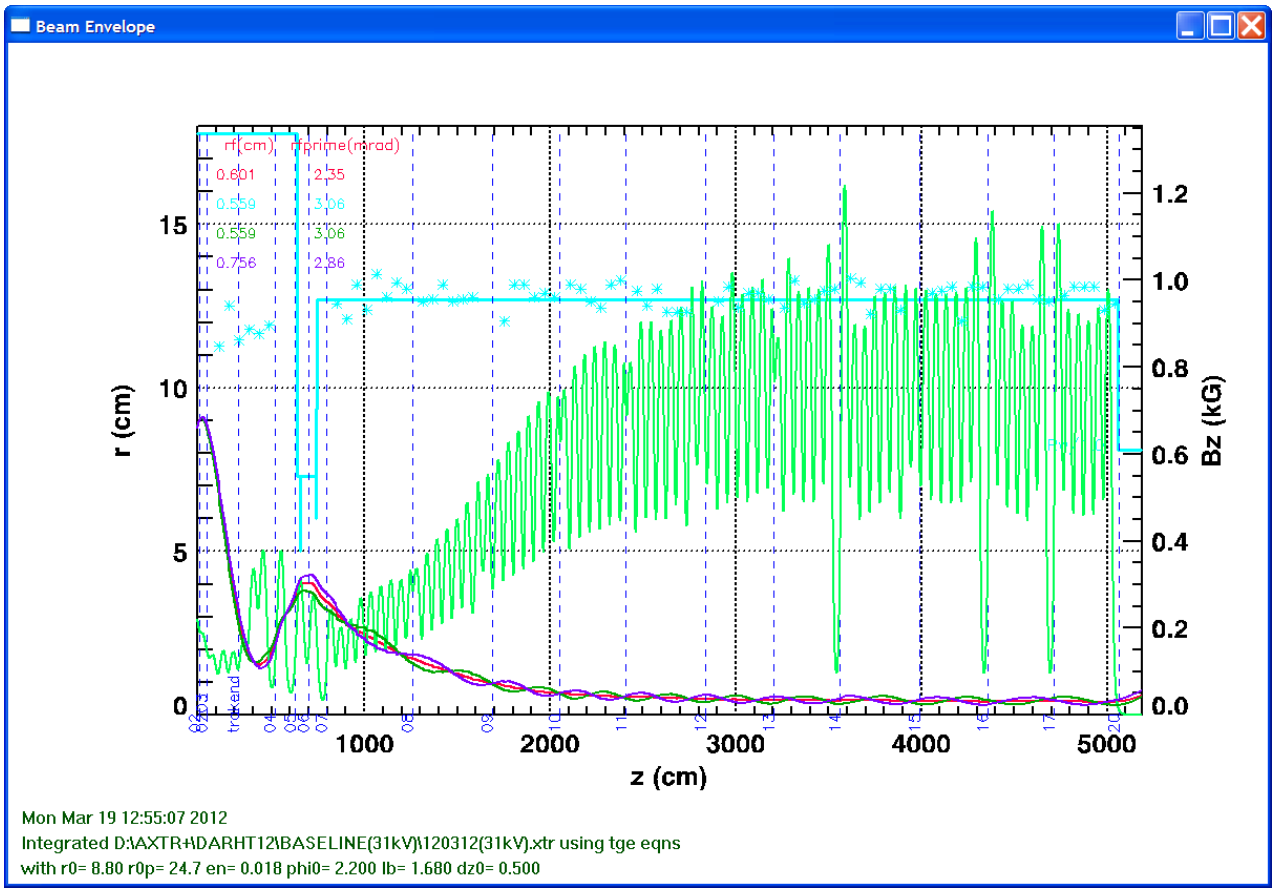

Figure 11: The red curve is the matched beam envelope with this tune for 1.68-kA initial conditions. Also shown are mismatched beam envelopes corresponding to the +/-2% uncertainty in the current measurement. The dark blue curve is the envelope for 1.71-kA initial conditions, and the dark green curve is the envelope for 1.66-kA initial conditions.

B. Focusing Solenoid Variations

Sensitivity to uncertainties in the solenoidal focusing fields was tested in two ways. First, the solenoid currents in XTR runs ware varied randomly. Second, the solenoid currents were varied coherently (ganged). The emittance growth was estimated by using the calculated envelope oscillation amplitude in the Slice interpolating formula.

Random variations: The solenoid currents were varied with perturbations having a normal distribution. Variations with standard deviations greater than 10% are unlikely, and were not considered. Because of the stochastic nature of these perturbations there is no strong correlation between strength of perturbation and resulting envelope oscillation amplitude, but some general features were noted. For random variations <10% the beam transported with envelope oscillations having a maximum envelope radius <1.1 cm, and peak-to-peak relative amplitude $A < 1.6$. Using the Slice interpolating formula for emittance growth, this could result in as much as 3000 π-mm-mr at the exit. On the other hand, for standard deviations less than ~4%, the predicted emittance growth was less than ~100 π-mm-mr. The greatest sensitivity is to variations in the injector solenoids. Indeed, if only the main LIA solenoids (cell07 – cell74) were allowed to vary, the predicted emittance growth was less than~300 π-mm-mr, even for as much

as 10% standard deviation. The conclusion is that this tune is insensitive to the sort of random uncertainties that might be expected in practice (standard deviation <4%).

Coherent variations : Predicted emittance growth due to coherent (ganged) variations of solenoid currents was strongly correlated with the strength of the variation. Figure 12 shows how the predicted emittance growth increases with changes in magnet currents from their nominal values. Again, beam envelope was least sensitive to variations in the main accelerator.

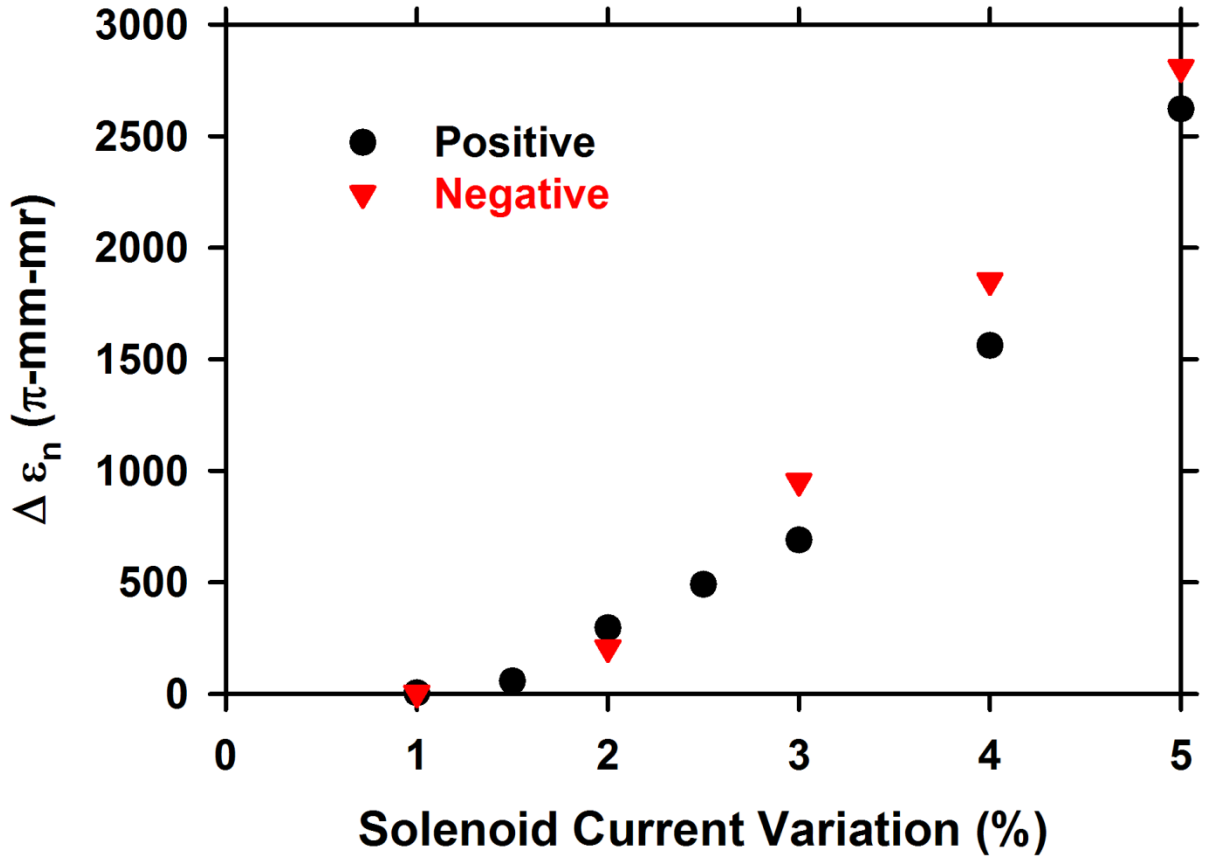

Figure 12: Predicted increase in emittance as a function of the variation of solenoid currents from the tune value. For this plot, all solenoid currents were changed by the same fractional amount (coherently). The filled circles represent positive changes, and the triangles represent negative changes.

C. Pulsed Power Variations

The tune is insensitive to random variations in the accelerating gap potentials. For example, a random variation of cell voltages with 10% standard deviation produced envelope oscillations with relative amplitude of only ~11%. However, 10% coherent variation of gap potentials produced ~32% envelope oscillations, which is just at the threshold of observable emittance growth.

VI. Conclusions

A new tune for the DARHT Axis-II focusing solenoids was designed and analyzed using several beam dynamics codes. The tune is based on more reliable estimates of initial parameters out of the diode, and provides a slightly better balance between BBU and corkscrew. This tune retains previous settings for the injector solenoid currents, although the steering dipoles may require slight adjustment to better center the beam. The beam dynamics for this tune meets all of the long-standing requirements for DARHT, based on simulations performed with beam envelope, ray-tracing, and particle-in-cell codes. The tune is robust to experimental uncertainty and perturbations. Simulations show only minimal emittance growth resulting from realistic uncertainties in values used for initial parameters, solenoidal focusing, or accelerating potentials.

In the absence of beam-target interactions, emittance is the limiting factor for radiographic source spot size and resolution. Since emittance growth feeds on envelope oscillation amplitudes, my tunes have all been designed to minimize oscillations by matching the solenoidal focusing to the injected beam. Moreover, adjustment of just a few solenoids can re-match the tune, should initial conditions, or other parameters, slightly change. What is needed to take full advantage of this feature is an emittance monitor at the accelerator exit, ahead of the complications introduced by the downstream transport. Of course, the ideal emittance monitor would be real-time, and non-invasive.

VII. Acknowledgements

The author acknowledges many interesting discussions with his colleagues, especially with Kurt Nielsen, B. Trent McCuistian, David Moir, Chris Rose, and Martin Schulze. This work was supported by the US National Nuclear Security Agency and the US Department of Energy under contract W-7405-ENG-36.

REFERENCES

[1] Carl Ekdahl, et al., “First beam at DARHT-II,” in Proc. 2003 Part. Accel. Conf., (2003), pp. 558-562.

[2] Carl Ekdahl, et al., “Initial electron-beam results from the DARHT-II linear induction accelerator,” IEEE Trans. Plasma Sci., vol. 33, (2005), pp. 892-900.

[3] Carl Ekdahl, et al., “Long-pulse beam stability experiments on the DARHT-II linear induction accelerator,” IEEE Trans. Plasma Sci. , vol. 34, (2006), pp.460-466.

[4] Carl Ekdahl, et al., “Suppressing beam-centroid motion in a long-pulse linear induction accelerator,” Phys. Rev. Special Topics-Accelerators and Beams, vol. 14, (2011) 120401.

[5] Martin Schulze, et al., “Commissioning the DARHT-II Accelerator Downstream Transport and Target,” in Proc. 2008 Linear Accel. Conf., (2008) , pp. 427-429.

[6] E. P. Lee and R. K. Cooper, “General envelope equation for cylindrically symmetric charged-particle beams,” Part. Acc. , vol. 7, (1976), pp. 83-95.

[7] P. Allison, “XTR, a new beam dynamics code for DARHT,” DARHT Tech Note #50, unpublished, (1995).

[8] Thomas P. Hughes, David C. Moir, and Paul W. Allison, “Beam injector and transport calculations for ITS,” in Proc. 1995 Part. Accel. Conf., (1995), pp. 1207-1209.

[9] Thomas C. Genoni, Thomas P. Hughes, and Carsten H. Thoma, "Improved envelope and centroid equations for high current beams", AIP Conf. Proc., vol. 650, (2002), p. 463.
[10] Thomas P. Hughes, et al., "LAMDA User's Manual and Reference", Voss Scientific technical report VSL-0707, April 2007.
[11] T. P. Hughes, R. E. Clark, and S. S. Yu, "Three-dimensional calculations for a 4 kA, 3.5 MV, 2 microsecond injector with asymmetric power feed," Phys. Rev. Special Topics- Accel. Beams, vol. 2, (1999), pp. 110401-1 – 110401-6.
[12] Stanley Humphries Jr., "TRAK – Charged particle tracking in electric and magnetic fields," in Computational Accelerator Physics, R. Ryne Ed., New York: American Institute of Physics, (1994), pp. 597-601.
[13] Technical information about the TriComp series of codes is available at www.fieldp.com.
[14] Stanley Humphries Jr., *Field solutions on computers,* (CRC Press Boca Raton, FL 1997) and www.fieldp.com.
[15] Carl Ekdahl, "Beamline tunes for DARHT-II Phase-1 commissioning," DARHT Tech. Note #252 and Los Alamos National Laboratory Report LA-UR- 02-3921, (2002).
[16] C. D. Child, "Discharge for hot CaO," Phys. Rev., vol. 32, 1911, pp. 492-511.
[17] I. Langmuir, "The effect of space charge and residual gases on thermionic currents in high vacuum," Phys. Rev., Second series,vol. 2, 1913, pp. 450-486.
[18] I. Langmuir, "The effect of space charge and initial velocities on the potential distribution and thermionic current between parallel plane electrodes," Phys. Rev., vol. 21, 1923, pp. 419-435.
[19] M. Reiser, *Theory and design of charged particle beams,* (Wiley, New York, NY 1994) p. 467 *et seq.*
[20] C. Thoma, and T. P. Hughes, "A beam-slice algorithm for transport of the DARHT-2 accelerator," in Proc. 2007 Part. Accel. Conf., (2007), pp. 3411-3413.
[21] T. P. Wangler, et al., "Particle-core model for transverse dynamics of beam halo," Phys. Rev. Special Topics- Accel. Beams, vol. 1, (1998), p. 084201.
[22] R. L. Guckstern, "Analytic model for halo formation in high current ion linacs," Phys. Rev. Lett., vol. 73, (1994), p. 1247.
[23] V. K. Neil, L. S. Hall, and R. K. Cooper, "Further theoretical studies of the beam breakup instability," Particle Accelerators, vol. 9, (1979), pp. 213-222.
[24] Y.-J. Chen, "Corkscrew modes in linear accelerators," Nucl. Instr. and Meth. in Phys. Res., vol. A 292, (1990) pp. 455-464
[25] T. Houck, LBNL Engineering Note M8109, June 6, 2002; DARHT Technical Note 257, August 19, 2002; and Personal Communications, 2001-2004
[26] M. Schulze, Personal communication, August 11, 2009
[27] M. Reiser, "Laminar-flow equilibria and limiting currents in magnetically focused electron beams," Phys. Fluids, vol. 20 (1977) p. 477
[28] P. Allison, "Beam dynamics equations for XTR," DARHT Tech Note #226, Los Alamos National Laboratory Report LA-UR-01-6585 (2001).
[29] Carsten Thoma, Thomas P. Hughes, and Craig Miller, "Envelope and centroid equations in LAMDA and XTR codes," Voss Scientific technical report VSL-0808, March 2008.
[30] C.A. Ekdahl, "Modeling Ion-Focused Transport of Electron Beams With Simple Beam-Envelope Simulations," Sandia National Laboratory Report, SAND-0544, 1986 (Available from National Technical Information Service DE86012739)
[31] S. Humphries, Jr., *Charged particle beams,* (Wiley, New York, 1990)
[32] P. Loschialpo, et al., "Effects of space charge and lens aberrations in the focusing of an electron beam by a solenoid lens," J. Appl. Phys., vol. 57, (1985) pp. 10-17.

[33] S. Bernal, et al., “Edge imaging in intense beams,” Phys. Rev. –STAB , vol. 5, (2002) p. 064202

Appendix A

DARHT Axis-II Accelerator Solenoid Magnet Settings

XTR Tune = D:\AXTR+\DARHT12\BASELINE(31kV)\120312(31kV).xtr

(31kV) nu PP+nu IC (from 2/16/12 data), bad mags 21,24,26,43,67,72,73 modeled, 53=OK

Solenoid Name	Current (A)
Diode	
Bucking Coil	12.060 (equivalent
Anode 1	7.5890
Anode 2	7.3440
Anode 3	18.814
Cell Block 1 (Injector)	
1	1.894 A
2	2.275 A
3	2.252 A
4	2.642 A
5	5.367 A
6	6.325 A
BCUZ	
BCUZ 1	6.962 A
BCUZ 2	5.651 A
BCUZ 3	4.936 A
Cell Block 2	
7	3.534 A
8	2.902 A
9	3.175 A
10	3.909 A
11	4.098 A
12	4.298 A
13	4.509 A
14	4.425 A
Inter Cell	3.641 A

Cell Block 3

15	4.681 A
16	5.392 A
17	5.857 A
18	6.178 A
19	6.423 A
20	6.667 A

Ext Int Cell 8.656 A

Ext Int Cell 8.970 A

Cell Block 4

21	9.528 A
22	8.978 A
23	9.457 A
24	10.775 A
25	10.469 A
26	11.485 A

Inter Cell 8.002 A

Cell Block 5

27	10.409 A
28	11.663 A
29	12.056 A
30	12.308 A
31	12.476 A
32	12.158 A

Inter Cell 8.855 A

Cell Block 6

33	11.276 A
34	13.148 A
35	13.106 A
36	12.770 A
37	12.984 A
38	12.843 A

Ext Int Cell 16.001 A

Ext Int Cell 16.196 A

Cell Block 7

39	12.572 A
40	13.098 A
41	14.774 A
42	14.000 A
43	16.999 A
44	14.320 A

Inter Cell 10.268 A

Cell Block 8

45	11.991 A
46	15.308 A
47	14.129 A
48	14.275 A
49	14.179 A
50	15.956 A

Cell Block 9

51	18.046 A
52	12.957 A
53	12.957 A
54	13.917 A
55	13.917 A
56	13.500 A

Ext Int Cell 16.121 A

Ext Int Cell 15.913 A

Cell Block 10

57	13.178 A
58	13.860 A
59	13.988 A
60	14.104 A
61	14.223 A
62	16.188 A

Cell Block 11

63	17.127 A
64	13.836 A
65	13.819 A
66	13.015 A
67	21.531 A
68	16.626 A

Cell Block 12

69	16.688 A
70	13.507 A
71	13.404 A
72	14.239 A
73	16.178 A
74	14.437 A

Appendix B

Simulation code comparisons

Designing a tune for DARHT relies heavily on a number of beam dynamics simulation codes. This appendix covers a few details and comparisons between these codes that were not covered in the main text.

1. XTR and LAMDA

XTR and LAMDA are both envelope codes. XTR was written at LANL by Paul Allison [28] at the same time (1990s) as LAMDA was written at MRC by Tom Hughes and coworkers [29]. There was extensive collaboration between the code authors in an effort to ensure that same physics was included in both codes, so it should be no surprise that there has always been good agreement between them. More recently, XTR was upgraded to use the same envelope equations contained in the most recent version of LAMDA [9] as an option, so that the LIA simulations with XTR would be consistent with DST simulations using LAMDA. Thus, the excellent agreement between recent XTR and LAMDA simulations is essentially a comparison of numerical techniques and their implementation. It is more enlightening to compare the earlier XTR (and LAMDA) envelope solutions [28], which were based on Reiser's theory [27] of an equilibrium beam produced by a shielded source; one with no magnetic flux linking the cathode surface. An example comparison for is shown for XTR in Fig. B2. The red curve is a calculation of the envelope for the tune described in this article using the most modern envelope equations [9]. The envelope calculated using the earlier equations (blue curve) exhibits mild oscillations.

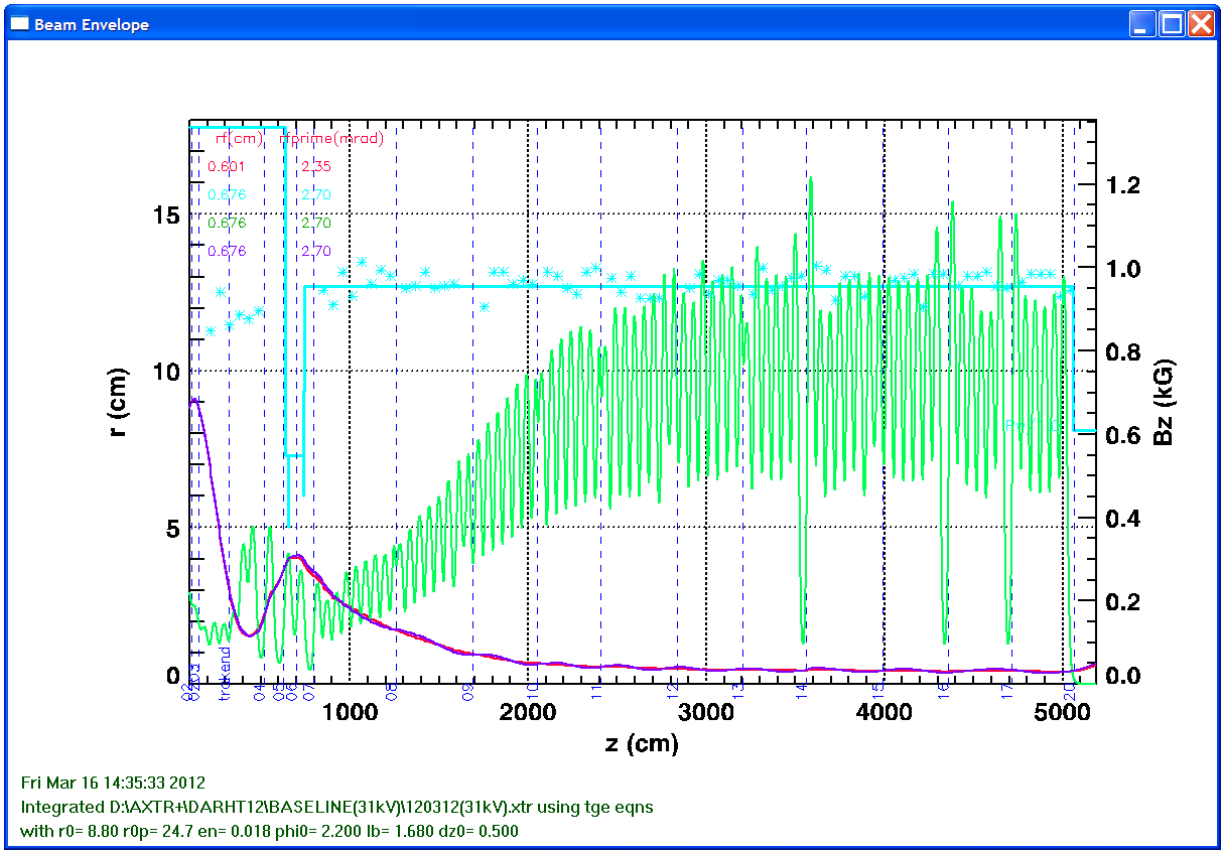

Figure B2: The red curve is a calculation of the envelope for the tune described in this article using the most modern envelope equations incorporated in XTR and LAMDA [9]. The envelope calculated using the earlier equations [28] (blue curve) exhibits mild oscillations.

Appendix C

Beam envelope equations

A convenient way to treat the transport of a high current electron beam is through the use of an envelope equation, which describes the beam size as a function of axial position, *z*. These have been derived in a number of ways, for various beam current distributions [6,7,9,19,31]. For simplicity, consider a uniform density-profile beam with radius $a(z)$ propagating in the z direction through a beam pipe with solenoidal magnetic focusing with axial field B_z on axis. To first order, the beam envelope equation can then be written as

$$\frac{d^2a}{dz^2} = -\frac{1}{\beta^2\gamma}\frac{d\gamma}{dz}\frac{da}{dz} - \left\{\frac{1}{2\beta^2\gamma}\frac{d^2\gamma}{dz^2} + k_\beta{}^2\right\}a + \frac{K}{a} + \frac{\varepsilon^2 + \left(P_\theta / \beta\gamma m_e c\right)^2}{a^3} \tag{2}$$

Here, $\beta = v_e / c$, $\gamma = \sqrt{1 - 1/\beta^2} = 1 + KE / m_e c^2$, and the canonical angular momentum is $P_\theta = \gamma m_e a^2 \omega - eaA_\theta$, where the solenoidal vector potential is $A_\theta = aB_z / 2$. The solenoidal focusing term in Eq. (2) is

$$k_\beta^2 = \left(\frac{2\pi B_z}{\mu_0 I_A}\right)^2 \tag{3}$$

where the Alfven limiting current is

$$I_A = \frac{4\pi}{\mu_0}\frac{m_e c}{e}\beta\gamma = 17.08\beta\gamma \text{ kA} \tag{4}$$

There is additional focusing by the accelerating cell potentials

$$k_\gamma^2 = \frac{1}{2\beta^2\gamma}\frac{d^2\gamma}{dz^2} \tag{5}$$

so the total focusing is $k^2 = k_\gamma^2 + k_\beta^2$.

In Eq. (2), space-charge defocusing is accounted for in the generalized perveance, which is $K = \left(2 / \beta^2\gamma^2\right)\left(\nu / \gamma\right)$ for a beam in vacuum, where, $\nu / \gamma = I_b / I_A$ is the Budker parameter, which is usually small in our LIA.

The DARHT injectors use reversed solenoids (bucking coils) to null the magnetic field at the electron source, so that $P_\theta = 0$ there. Since P_θ is conserved as the beam is transported through the accelerator (Buch's theorem) the defocusing of the last term in Eq. (2) is due to the emittance alone. Moreover, since the solenoidal vector potential is non-zero in the focusing field, the beam rotates at the betatron frequency $\omega = \omega_\beta = eB_z / 2\gamma m_e$ in the LIA. Because of this

rotation x and y are coupled, and care must be taken when defining the emittance in the cylindrical coordinate system used for Eq. (2),

$$\varepsilon^2 = 4\left(\left\langle r^2\right\rangle\left[\left\langle r'^2\right\rangle + \left\langle \left(r\omega/\beta c\right)^2\right\rangle\right] - \left[\left\langle rr'\right\rangle^2 + \left\langle r^2\omega/\beta c\right\rangle^2\right]\right) \tag{6}$$

It is only for a drifting, non-rotating, circular beam that the emittance is simply $\varepsilon = 4\varepsilon_x = 4\varepsilon_y$, where $\varepsilon_x = \sqrt{\left\langle x^2\right\rangle\left\langle x'^2\right\rangle - \left\langle xx'\right\rangle^2}$, etc. (In these equations, the bracket symbol $\langle\ \rangle$ denotes moments of the quantities over the six-dimensional particle distribution in position and velocity.)

As written, Eq. (2) applies to a beam with a uniform current density. However, it is completely equivalent to Ed Lee's derivation [9] of the equation for the rms radius R_{rms} of an arbitrary azimuthally symmetric current density distribution. One only need substitute $a = \sqrt{2}R_{rms}$, where $R_{rms} = \sqrt{\left\langle r^2\right\rangle}$. Thus, the radius a can always be considered an "equivalent envelope" radius for any azimuthally symmetric current distribution, and Eq. (2) can be used as written.

Equation (2) is integrated in simulation codes to find the beam envelope radius $a(z)$ under various physical approximations [7-10, 29, 30]. Chief among those are an approximation to the space-charge depression of the beam kinetic energy, and an approximate correction to the applied magnetic field to account for the beam diamagnetism [7, 9].

Finally, some envelope codes simulate a propagating current pulse by breaking the pulse up into independent disks (each with their own current, energy, emittance, and initial conditions) and then solving the envelope equation for each disk [9, 10, 29, 30].

Appendix D

Particle-in-cell (PIC) simulations

A mismatched beam is characterized by envelope oscillations. The free energy of these oscillations feeds the growth of emittance [19]. One mechanism of emittance growth is parametric amplification of resonant electron orbits, expelling electrons from the beam core into a halo [21]. This effect, and the resultant emittance growth, can be simulated with a particle-in-cell (PIC) code. For these simulations, I used a beam slice algorithm for the LSP PIC code that was developed specifically for DARHT Axis-II [20]. Two slice models have been used; Slice 1D models a centered beam in cylindrical coordinates, while Slice2D uses Cartesian coordinates in order to incorporate motion of the beam centroid.

Slice propagates a transverse slice of the beam through the stationary focusing and accelerating fields, incrementing the transverse equations of motion for the particles at each time step. The solenoidal focusing magnetic field is taken from the on-axis values used in Slice is initiated at the diode exit, at a point where the beam envelope is at a maximum (no divergence). The slice is launched as a uniform beam rotating rigidly in the magnetic field with stochastic emittance added. For the new tune the launch point is at z=125.3 cm, which is slightly downstream of the z=100-cm location of handoff from TRAK to XTR. The initial parameters for the slice simulations were taken from XTR simulations.

Figure D1 shows a comparison of the matched beam envelope modeled by the two versions of slice, and the XTR envelope code.

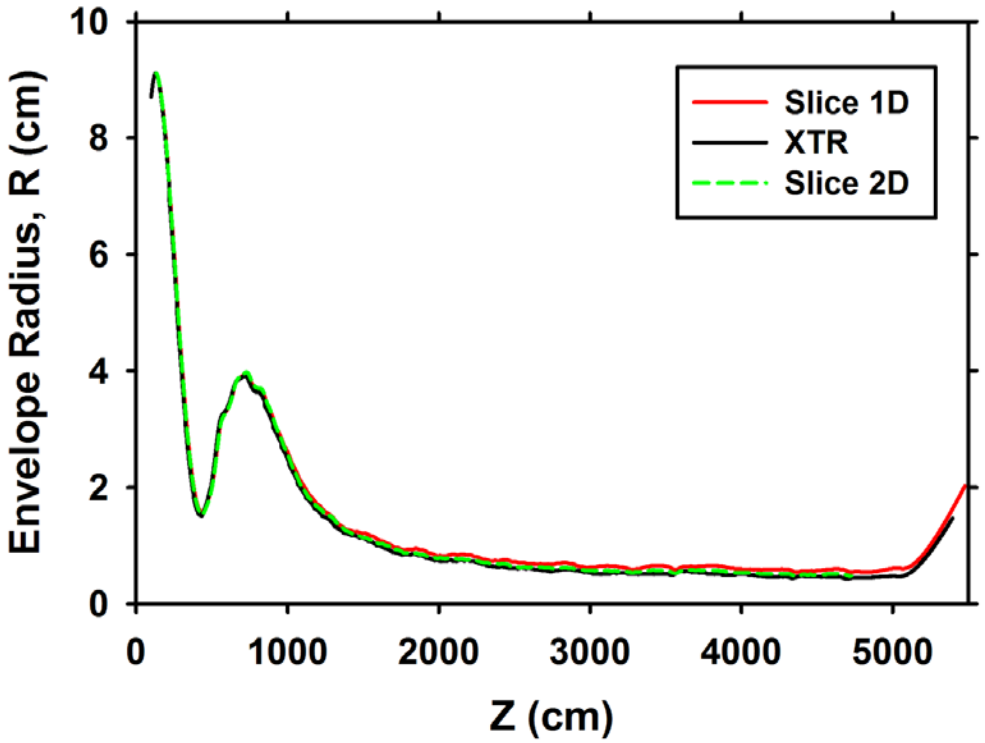

Figure D1: Beam envelope modeled by the two versions of the LSP Slice code and the XTR envelope code.

In order to illustrate the mechanism for emittance growth in a mismatched beam, I performed a 2D simulation with the beam on axis, but with a ~10% incorrect initial envelope radius. The

resulting beam envelope and emittance growth are shown in Fig. D2. Figure D3 shows snapshots of the beam phase and configuration space at four different locations (as indicated in Fig. D2).

These simulations of emittance resulting from beam halo are corroborated by early measurements on the D2 accelerator [2]. In those experiments extremely mismatched beams with substantial halo and very high emittance resulted from an incorrect cathode geometry. The fact that beam emittance is the result of halo production rather than increase in the stochastic motion makes it possible to substantially reduce emittance by passing the beam through an emittance filter consisting of an aperture that scrapes off the halo. There would be little current loss. For example, as described in Ref. 2, even in extreme cases only~20% of the beam current is carried in the halo, which contributes ~76% of the emittance.

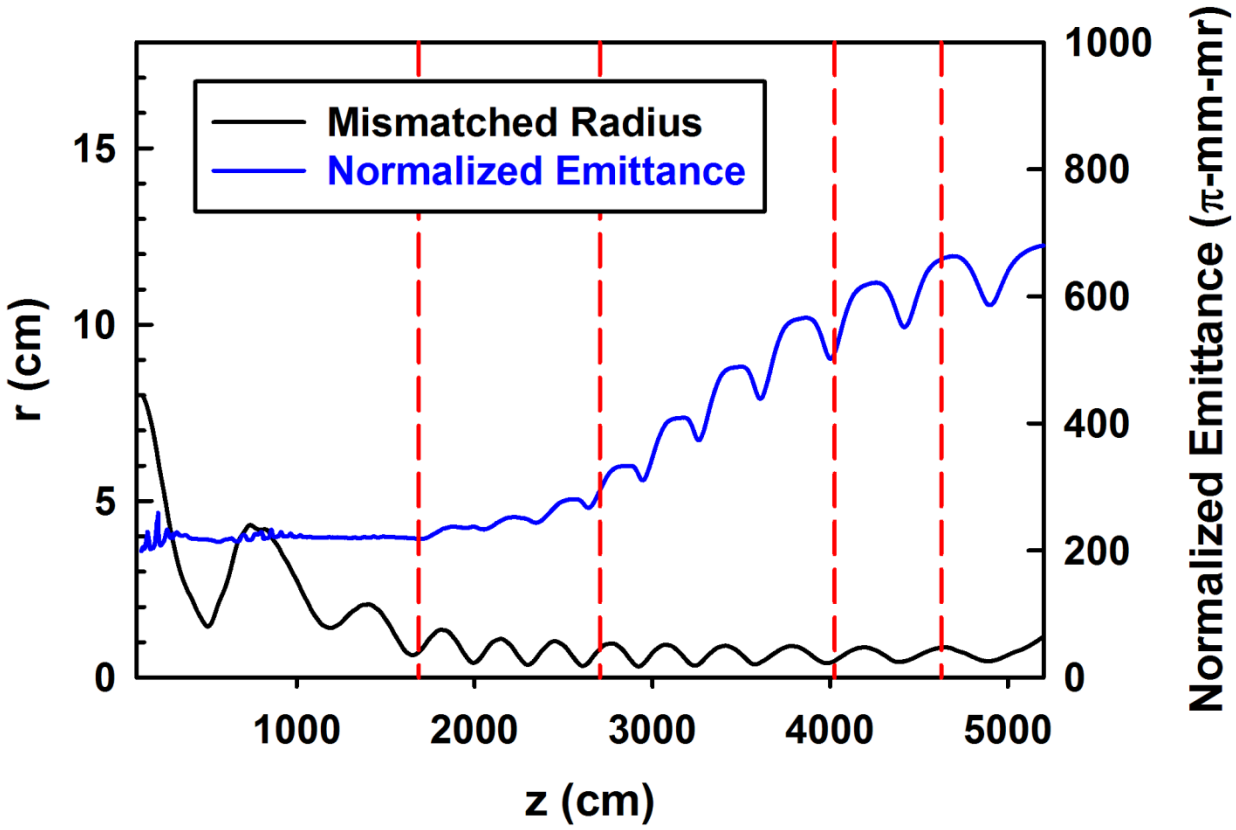

Figure D2: Slice_2D simulations of a beam that was mismatched by setting the initial envelope radius 10% less than for a matched beam. The vertical dashed red lines indicate the positions of the snapshots in Fig. D3.

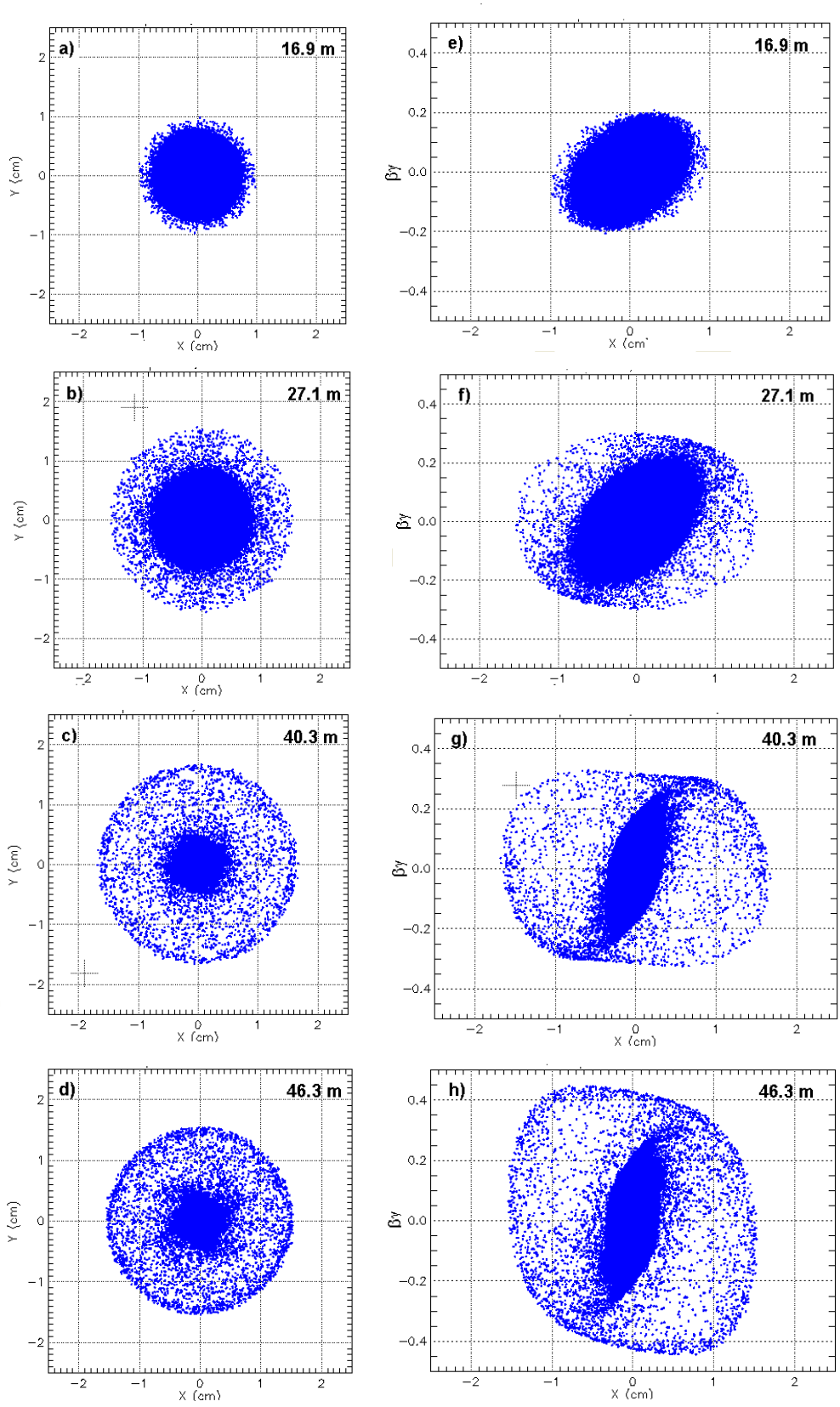

Figure D3: Left column (a, b, c, d): Configuration space showing growth of halo as mismatched beam propagates through LIA. Right column (d, e, f, g): Phase space showing resonant particle ejection into the halo, with large momentum (βγ) contribution to emittance.